Intracellular Assembly of Interacting Enzymes Yields Highly-Active Nanoparticles for Flow Biocatalysis

Patrick Bitterwolf,[a] Ahmed E. Zoheir,[b] Julian Hertel,[a] Sandra Kröll,[a] Kersten S. Rabe,[a] and Christof M. Niemeyer*[a]

Abstract: All-enzyme hydrogel (AEH) particles with a hydrodynamic diameter of up to 120 nm were produced intracellularly with an *Escherichia coli*-based in vivo system. The inCell-AEH nanoparticles were generated from polycistronic vectors enabling simultaneous expression of two interacting enzymes, the *Lactobacillus brevis* alcohol dehydrogenase (ADH) and the *Bacillus subtilis* glucose-1-dehydrogenase (GDH), fused with a SpyCatcher or SpyTag, respectively. Formation of inCell-AEH was analyzed by dynamic light scattering and atomic force microscopy. Using the stereo-selective two-step reduction of a prochiral diketone substrate, we show that the inCell-AEH approach can be advantageously used in whole-cell flow biocatalysis, by which flow reactors could be operated for >4 days under constant substrate perfusion. More importantly, the inCell-AEH concept enables the recovery of efficient catalyst materials for stable flow bioreactors in a simple and economical one-step procedure from crude bacterial lysates. We believe that our method will contribute to further optimization of sustainable biocatalytic processes.

Introduction

Spatial arrangement of biomolecules is a key fundamental principle of cellular life and offers a plethora of possibilities for enhancing reactions in multienzyme biocatalysis for the production of value-added compounds or fine and bulk chemicals by using isolated enzymes or whole cells.[1] Following nature's example, many approaches are being taken to spatially organize enzymes by using protein fusions,[2] bacterial microcompartments,[3] the formation of functional inclusion bodies,[4] or molecular scaffolding systems based on proteins,[5] peptides,[6] DNA[7] or RNA.[8] Due to the spatial proximity of the enzymes resulting from the supramolecular structure, substrates can be more efficiently converted, allowing for quick depletion of intermediates and preventing crosstalk with competing reactions in the surrounding bulk solution.[9] However, simple enzyme fusion often results in decreased catalytic activity and scaffold-mediated systems hold several drawbacks like uncontrolled aggregation due to oligomerization of enzymes.[10]

Therefore, there is a high demand for new approaches to prepare efficient catalytically active materials for multi-enzyme synthesis.

With the purpose to overcome such limitations, we have recently developed a site-specific method for enzyme assembly that is based on SpyCatcher (SC)/SpyTag (ST) conjugation to produce in vitro self-assembling all-enzyme hydrogels (AEH) and enables full control over the relative stoichiometry of the binding partners.[11] The SC/ST system, originating from *Streptococcus pyogenes*, is a split-engineered two-component protein coupling system capable of rapid covalent binding under physiological conditions forming a stable isopeptide bond.[12] We demonstrated that the AEH approach could be applied to (R)- & (S)- stereoselective alcohol dehydrogenases as well as imine reductases and decarboxylases, thus offering a versatile toolbox for assembly and immobilization of biocatalytic AEH materials which enabled the production of microfluidic reactors that proved to be stable for tens of days under continuous perfusion conditions.[11,13]
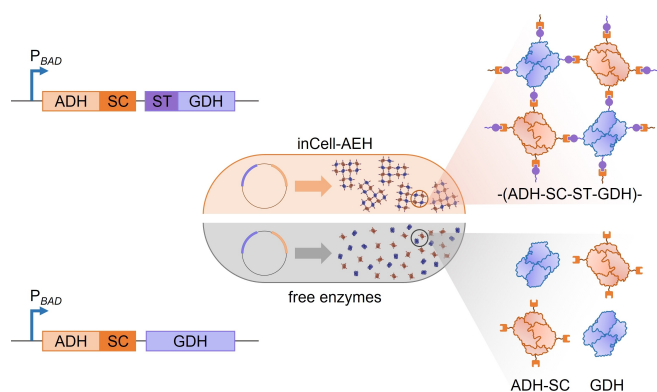
Since our AEH design can be readily applied to multiple classes of enzymes, we wanted to explore the possibilities of producing these materials in living cells for use in diverse flow biocatalysis formats. Previous examples of SC/ST-mediated enzyme conjugation in living bacteria were limited to co-expression of bacterial microcompartment shells,[14] compartment-forming mediators such as elastin-like protein[15] or the crystallizing Cry protein,[16] or resulted in uncontrolled formation of inclusion bodies that must be further stabilized by chemical cross-linking.[17] Therefore, to enable independently controllable bifunctional enzyme aggregation in *E. coli*, in this work polycistronic vectors were cloned containing genes encoding for a (R)-stereoselective alcohol dehydrogenase (ADH) and a glucose-1-dehydrogenase (GDH) fused with SC and ST domains, respectively (Figure 1). We demonstrate that *E. coli* cells trans-

[a] Dr. P. Bitterwolf, J. Hertel, S. Kröll, Dr. K. S. Rabe, Prof. C. M. Niemeyer
Institute for Biological Interfaces (IBG1)
Karlsruhe Institute of Technology (KIT)
Hermann-von-Helmholtz-Platz 1, Karlsruhe, 76344 (Germany)
E-mail: niemeyer@kit.edu

[b] Dr. A. E. Zoheir
Department of Genetics and Cytology
National Research Centre (NRC)
33 El Buhouth St., Cairo, 12622 (Egypt)

Chem. Eur. J. **2022**, 28, e202202157 (1 of 7)

© 2022 The Authors. Chemistry - A European Journal published by Wiley-VCH GmbH

Chemistry–A European Journal

Research Article
doi.org/10.1002/chem.202202157

**Chemistry
Europe**
European Chemical
Societies Publishing

Figure 1. Schematic representation of the inCell-AEH design. *E. coli* cells express SpyCatcher-tagged ADH (ADH-SC) and SpyTag-modified GDH (GCH-ST) under an arabinose inducible promotor (P_{ara}). Spontaneous formation of a covalent isopeptide bond between SC and ST leads to formation of intracellular all-enzyme hydrogels (inCell-AEH). For control purposes, *E. coli* cells were used that express the ADH-SC together with an untagged version of GDH lacking the SpyTag, thereby preventing the formation of inCell-AEH materials.

formed with these vectors can express the two corresponding coupling partners to form intracellular multienzyme complexes with submicron dimensions, hereafter referred to as inCell-AEH. We show that the inCell-AEH materials can be used in both batch and flow-through reaction systems to enable a stereoselective reduction cascade with regeneration of the cofactor NADPH. In addition, the inCell-AEHs can be used from crude bacterial lysates through a convenient one-step procedure for purification and co-immobilization of equimolar amounts of enzymes.

Results and Discussion

For the design of the inCell-AEH, two enzymes were chosen. The (*R*)-stereoselective alcohol dehydrogenase ADH (EC 1.1.1.2) from *Lactobacillus brevis*, capable of stereoselective reduction of prochiral ketones,[18] was combined with cofactor NADPH regenerating enzyme glucose-1-dehydrogenase GDH (EC 1.1.1.118) from *Bacillus subtilis*.[19] ADH and GDH were genetically fused with the SpyCatcher (SC) and SpyTag (ST) coupling elements (Figure 1), in addition to a hexahistidin tag for purification. Since both enzymes have a homotetrameric quaternary structure, tetravalent building blocks are formed that can polymerize into multienzyme complexes. For control, a plasmid was designed where only ADH was tagged with SC but the GDH was lacking the corresponding ST to prevent polymerization of multienzyme complexes. The genes encoding for the enzymes in the inCell-AEH and control vectors were assembled polycistronic behind an L-arabinose inducible promotor (P_{BAD}).[20] For each encoded protein a ribosome binding site sequence (RBS) was placed directly upstream of ADH and GDH to ensure that the proteins were expressed individually and in equal

stoichiometric ratio (for plasmid maps, see Figure S1, in the Supporting Information).

To investigate whether cells that can produce the inCell-AEH have difficulties to grow after L-arabinose induction, OD_{600} growth curves were measured initially (Figure 2A). Before induction, no difference in growth was observed, whereas after induction the inCell-AEH expressing cells went faster in a stationary phase than the control cells expressing only unassembled free enzymes. To elaborate on the protein expression in the cells expressing inCell-AEH and control enzymes, SDS-PAGE analyses of crude lysates before and after affinity purification with Ni-NTA resin were performed (Figure 2B). The electrophoretic analysis revealed that both cell types expressed the enzymes ADH-SC (40 kDa) and GDH-ST (31 kDa)/GDH (29 kDa) as expected (lanes 1, 2 in Figure 2B). These findings were confirmed by Ni-NTA purification, which led to only free enzymes (lane 9) or the expected conjugation band (lane 10) in the case of the control and inCell-AEH samples, respectively. The analysis also revealed that slightly higher levels of GDH-ST/GDH than ADH-SC were expressed in both cell types. Presumably this is due to the fact that in both vectors GDH is located upstream of ADH on the polycistronic constructs, thereby leading to higher expression levels.

To investigate the size of the putative multienzyme complexes, we carried out dynamic light scattering (DLS) analysis of the Ni-NTA purified inCell-AEH and control lysates (Figure 2C). Indeed, we observed a significant about 3–4 fold
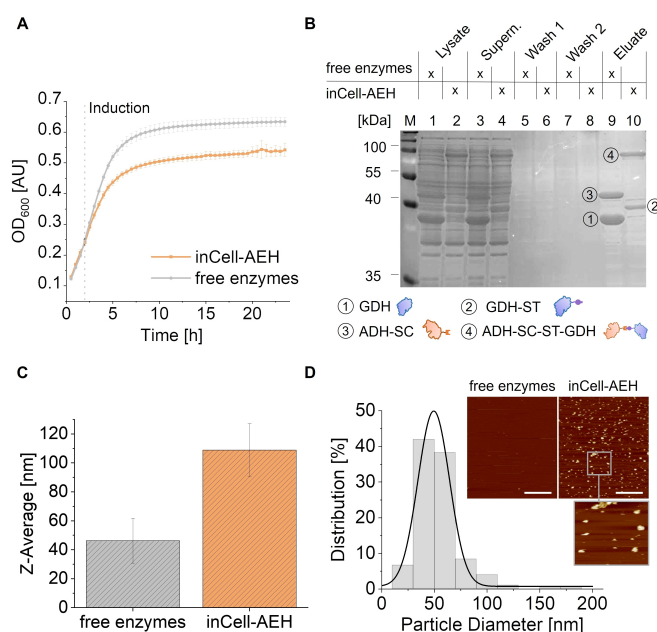

Figure 2. Characterization of cell growth and inCell-AEH formation. A) OD_{600} growth curves of *E. coli* cells expressing the inCell-AEH and control vectors. B) 15% coomassie stained SDS-PAGE analysis of lysed inCell-AEH and control cells before and after purification by Ni-NTA affinity chromatography. M: Thermo Scientific™ PageRuler Prestained Protein Ladder. C) DLS measurements of control and inCell-AEH protein samples subsequent to Ni-NTA purification. D) Particle diameter distribution of control and inCell-AEH protein samples determined by AFM subsequent to Ni-NTA purification. Scale bar: 600 nm.

Chemistry–A European Journal

Research Article
doi.org/10.1002/chem.202202157

Chemistry Europe
European Chemical
Societies Publishing

increase in the mean hydrodynamic particle size (Z-average), indicating that particles with a diameter of $> 0.12 \, \mu m$ were formed inside the cells. To further investigate the particle sizes, the Ni-NTA-purified proteins were additionally analyzed by atomic force microscopy (AFM) (Figure 2D). Compared to the free enzymes, the inCell-AEH samples showed a distribution of particle diameters in the range of 20–120 nm, which is in good agreement with the DLS data and indicates SC-ST-driven and thus controlled aggregation of the corresponding enzymes.

Since all protein expression studies were consistent with expectations, we then addressed the characterization of the biocatalytic properties of the two different cell types. To this end, we applied a two-step enzymatic cascade reaction taking advantage of the previously reported model system based on the prochiral substrate 5-nitrononae-2,8-dione **1** (NDK, Figure 3A).[18b] ADH-mediated reduction of **1** lead to formation of the (R)-configured syn- & anti-hydroxyketones **2a/2b**. In a second reduction step the remaining carbonyl group is reduced to form the corresponding (R,R)-configured diol **3**. To provide reducing agents for the ADH reactions, NADPH was generated from $NADP^+$ by GDH through oxidation of glucose to gluconolactone. All products were quantified by chiral HPLC analysis (Figure S2).

To enable optimal mass transfer of substrate **1** through the cell membrane, batch experiments were performed using whole cells treated with variable concentrations of toluene (Figure 3B),
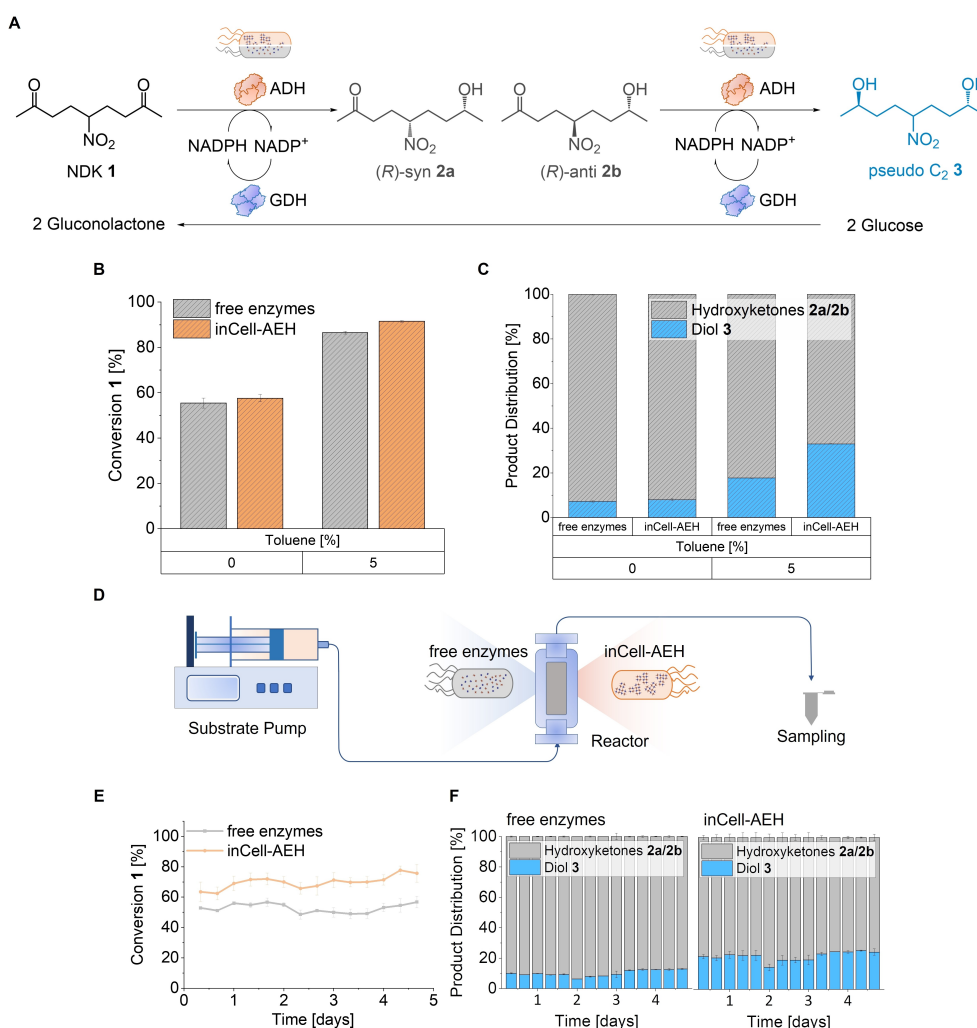
Figure 3. A) Reaction scheme of the biocatalytic reduction of 5-nitro nonane-2 8-dione (NDK; **1**) using ADH and GDH. The (R)-specific ADH converts NDK to the corresponding hydroxyketones **2a/2b** and in a subsequent second reaction step to the pseudo C_2 diol **3**. The ADH consumed cofactor NADPH is regenerated by means of GDH and glucose. B) Conversion of **1** to **2a/2b** and **3**, as determined by HPLC measurements of *E. coli* treated with 0 or 5% toluene for cell wall permeabilization. C) Normalized product distribution of hydroxyketones **2a/2b** and diol **3** obtained from cells treated with 5% toluene, as determined by HPLC analysis. D) Schematic representation of the fluidics setup used to perfuse and sample bioreactors containing whole cells expressing either inCell-AEH or unassembled enzymes. E) Conversion of **1** to **2a/2b** and **3**, determined in a long-term flow experiment using whole-cell bioreactors loaded with inCell-AEH (orange) or control (grey) cells. Note that the apparent parallel trend in the fluctuations of the two curves is likely due to the fact that both reactors were operated in parallel with the same fluidic setup and therefore were subject to the same slight changes in ambient conditions (especially temperature). F) Normalized product distribution of hydroxyketones **2a/2b** and diol **3** collected at variable time points. The bioreactors were perfused at a flow rate of 5 $\mu L*min^{-1}$ with a substrate mix containing 5 mM NDK **1**, 1 mM NADP+, and 100 mM Glucose. Samples were quenched in 7 M guanidinium chloride and analyzed by HPLC. Error bars indicate the deviation between independent duplicates.

Chemistry–A European Journal

Research Article
doi.org/10.1002/chem.202202157

Chemistry Europe
European Chemical
Societies Publishing

which is a well-known procedure for cell permeabilization.[21] To assess the biocatalytic activity, about $8*10^8$ cells were sedimented from growth medium, washed, treated with toluene and subsequently incubated with a substrate mix containing 5 mM NDK **1**, 1 mM $NADP^+$ and 100 mM Glucose in an aqueous buffer for 20 min. Samples were then analyzed by HPLC.

We found that the inCell-AEH cells treated with 5% toluene showed the highest conversion of NDK **1** at 90% with an excellent enantiomeric excess of >99%. Only a slightly higher conversion was visible for the inCell-AEH as compared to the control cells (Figure 3B). However, closer inspection of the product distribution revealed significant differences between the inCell-AEH and the control cells (Figure 3C). The amount of diol **3** was almost twice as high for the inCell-AEH as compared to the control cells and this effect occurred only in the permeabilized cells (right set of bars, in Figure 3C). As indicated by previous studies with AEH materials purified and assembled in vitro,[11] these observations are in agreement with the presence or absence of AEH in the inCell-AEH and control cells, respectively. The close proximity of the ADH and GDH enzymes leads to increased reaction rates for the second, diol-forming reduction step and this mechanism cannot work if the substrate concentrations and thus the overall reaction rate are low in the case of the non-permeabilized cells.

Since the cells treated with toluene showed near quantitative conversion of NDK in a batch process, further experiments were performed to investigate the biocatalytic efficiency and long-term stability in a continuous flow process (Figure 3D). To this end, a bioreactor was designed by Computer Aided Design (CAD) software and fabricated by micromilling from a polytetrafluorethylene (PTFE) material to yield a reaction chamber in which 100 μL of an *E. coli* cell suspension ($OD_{600} = 10$) could be trapped between two filter membranes placed on top and bottom of the cell slurry (see also Figure S3). The reactor was perfused with substrate solution containing NDK, $NADP^+$ and Glucose and samples of the outflow were automatically collected using a robotic system and subsequently analyzed by HPLC (Figure 3E). We observed that both the inCell-AEH and control cell-loaded reactors exhibited stable turnover rates for more than 4 days. The inCell-AEH reactor initially showed ~10% higher conversion rates than the control reactor, increasing over time to ~20% after 24 h.

We attribute the stronger decrease in activity in the control reactor to an increased wash-out of the isolated enzymes compared to the larger AEH particles. Similar to the batch reactions (Figure 3C), an altered product distribution was observed for the inCell-AEH reactor with approximately 2-fold higher amounts of diol **3** (Figure 3F), confirming the presence of the AEH particles. Hence, space-time-yields (STY) of 18.8 $g*L^{-1}*d^{-1}$ or 9.4 $g*L^{-1}*d^{-1}$ of product **3** were calculated for the inCell-AEH and control reactor, respectively.

While the above experiments suggested that the use of inCell-AEH offers little advantage over isolated expressed enzymes in the whole-cell format, the concept of intracellular enzyme aggregation allows for a very distinct advantage in the preparation of biocatalytic reactor materials directly from crude cell extracts. To test whether the inCell-AEH expressing cells can

be used for a one-step preparation of reactor materials, we used commercially available epoxide microparticles that were functionalized with an SC protein by chemical linkage.[22] The SC-coated microparticles were then used for extraction of crude lysates obtained from either inCell-AEH or control *E. coli* cells (Figure 4A). In the case of the inCell-AEH cells, both ADH and GDH enzymes can be co-immobilized directly on the microparticles due to the intracellular formation of AEH particles, whereas in the control samples no enzyme is captured due to the lack of the corresponding ST on GDH.

Lysate of cells expressing the control enzymes only led to a low biocatalytic activity of the loaded microparticles (blue line, in Figure 4B), which may result from non-specific adsorption on the surface. In contrast, the inCell-AEH samples showed quantitative conversion of **1** to diol **3** for >7 days, indicating successful and stable co-immobilization of ADH-SC and GDH-ST on the microparticles (Figure 4B, red line). The AEH-loaded microparticles were also evaluated for their catalytic activity in the flow-through setup at different flow rates from 5 to 500 μL*min^{-1} (Figure 4C). It was found that the microparticles remained stable in the reactor compartment even at elevated flow rates. Impressively high total STY for hydroxyketones **2a**/**2b** were reached at 500 μL/min with 555 $g*L^{-1}*d^{-1}$. However, the maximum STY for the two times reduced diol **3** was reached at 5 μL*min^{-1} with 61 $g*L^{-1}*d^{-1}$.

We note that the increased catalytic activity of AEH materials described here and previously is not necessarily due to substrate channeling. Hess and coworkers have shown that
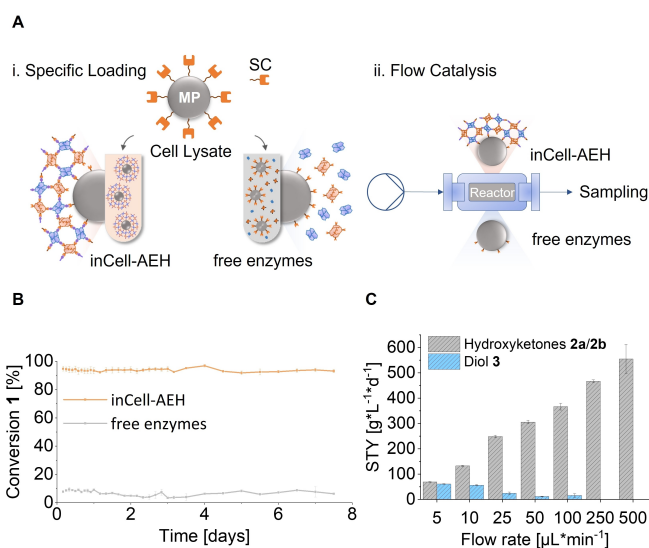
Figure 4. Direct purification of inCell-AEH yields biocatalytic reactor materials. A) Schematic illustration of the direct inCell-AEH immobilization on SC functionalized microparticles from crude cell lysates and subsequent integration in a flow bioreactor. Note that in the case of inCell-AEH cells both ADH and GDH enzymes are co-immobilized due to intracellular formation of AEH particles, whereas no enzyme is immobilized in the control samples (MP: Microparticle). B) Continuous flow conversion of a substrate mix (5 mM NDK **1**, 1 mM $NADP^+$, 100 mM Glucose) obtained at 5 μL*min^{-1} with SC-functionalized MP containing either inCell-AEH or free enzymes. C) Dependency of space-time-yields (STY) of hydroxyketones **2a**/**2b** (grey) and diol **3** (blue) from the flowrate. Samples were analyzed by HPLC. Error bars indicate the deviation between independent duplicates.

Chemistry–A European Journal

Research Article
doi.org/10.1002/chem.202202157

Chemistry Europe
European Chemical
Societies Publishing

proximity alone does not contribute to activity enhancement in a bienzymatic cascade,[23] which led them to emphasize that substrates in nature are channeled by confinement (compartmentalized reaction spaces with many catalytic centers) rather than proximity,[24] and to propose design principles for a compartmentalized enzyme cascade reaction.[25] We therefore hypothesize that the retention of cosubstrate and reaction intermediates observed in our studies is likely due to effects such as diffusion limitations in compartmentalized microenvironments present in AEH materials.

Conclusion

In conclusion, we have demonstrated for the first time that all-enzyme hydrogel (AEH) particles can be produced intracellularly with an *E. coli* based in vivo system. AEH nanoparticles with a hydrodynamic diameter of up to 0.12 μm containing equimolar amounts of co-localized enzymes were produced from plasmid vectors encoding for the enzymes ADH-SC and GDH-ST. Using the stereoselective two-step reduction of a prochiral diketone substrate, we show that the concept of intracellular AEH can be advantageously used in whole-cell flow-biocatalysis, where flow reactors could be operated for >4 days under constant substrate perfusion with maximum STY of up to 18.8 $g*L^{-1}*d^{-1}$. In addition, our inCell-AEH approach enables the co-immobilization of the interacting ADH/GDH enzymes in a simple and economically viable one-step procedure from crude bacterial lysates. This methodological approach is remarkable because it physically assembles multiple interacting enzymes in stoichiometrically tunable amounts, for example, by modifying the number of fused tags,[13a] and makes them amenable to easy isolation. Therefore, the method opens up numerous possibilities for the cascading of enzymes. Preliminary experiments indicate that the here described approach is applicable also to other interaction systems, such as the non-covalent binding system based on the GTPase-binding domain (GBD) with its corresponding ligand[26] (Figure S4). Since we have already shown that fabrication of the AEH materials is easily transferrable to other enzyme classes,[13] we believe that our work is broadly applicable and will contribute to the further optimization of sustainable biocatalytic processes.

Experimental Section

Construction of Plasmids: Genetic construction of the vectors for expression of the inCell-AEH and free enzymes was carried out using isothermal recombination described by Gibson et al. utilizing oligonucleotide primers with 30 bp homologous overlaps.[27] After PCR and assembly, reaction mixtures were treated with DpnI removing any remaining vector from prior PCR reactions. Subsequently, constructs were transformed into *E. coli* DH5α cells. Plasmids were purified using a ZR Plasmid Miniprep Classic Kit (Zymo Research, Germany) according to the manufacturer's instructions. Sequences were verified by commercial sequencing (LGC genomics, Germany). All primers used in this study are listed in Table S1.

For the Spy based vectors a pTF16 backbone with an encoded L-arabinose inducible promotor P_{BAD} was amplified using primer PB1_fwd and PB1_rev on template TP#17 to generate fragment#1. The sequence encoding BsGDH was amplified using primer PB2_fwd and primer PB2_rev on template TP#42 to generate fragment#2. The sequence encoding BsGDH-ST was amplified using the same primers PB2_fwd and PB2_rev on template TP#43 to generate fragment#3. The sequence encoding LbADH-SC was amplified with primer PB3_fwd and PB3_rev on template TP#47 to generate fragment#4. Subsequent to PCR amplification the fragments #1,3,4 and #1,2,4 were assembled by Gibson cloning to generate the vectors encoding for the inCell-AEH (TP#66) and free enzymes (TP#67), respectively (see Figure S1A & B).

For the GBD based vectors a pTF16 backbone with an encoded L-arabinose inducible promotor P_{BAD} was amplified using primer JH5_fwd and JH5_rev on template TP#67 to generate fragment #5. The gene fragment#6 encoding for the polycistronic inCell-AEH construct with BsGDH-GBDL and ADH-GBD was ordered by the Invitrogen GeneArt Strings DNA Fragments service of ThermoFisher Scientific. Subsequent to PCR amplification the fragments #5 & #6 were assembled by Gibson cloning to generate the vector PB#31 encoding for the inCell-AEH (Figure S1C). To generate the vector encoding for the free enzymes the GBDL tag was removed by PCR using the primers JH6_fwd und JH5_rev. Subsequently the fragment was circularized by Gibson assembly yielding the plasmid PB#34 (Figure S1D).

Growth Curves: For high resolution growth curves inoculation cultures were grown in Luria Bertani containing 25 μg*mL^{-1} chloramphenicol as selection marker (LB$_{Cm}$) at 37°C 180 rpm overnight. Overnight cultures were used to inoculate 5 mL LB$_{Cm}$ and grown to OD$_{600}$ 0.6–0.8. Subsequently, cultures were diluted to OD$_{600}$ 0.1 and transferred in a 96-well plate. Measurements were performed hourly with a Synergy H1 reader (BioTek Instruments, Germany) and after 3 h the cultures were induced with 5 mM arabinose.

Protein Expression: For heterologous expression *E. coli* BL21(DE) cells were transformed with plasmids pTF16_BsGDH_LbADH-SC (control) or pTF16_BsGDH-ST_LbADH-SC (inCell-AEH), respectively. Transformed cells were plated out and incubated over night at 37°C on LB$_{Cm}$ plates. For the inoculation culture transformed colonies were selected and used to inoculate 30 mL of liquid LB$_{Cm}$. The liquid cultures were grown for 16 h at 25°C and 180 rpm. Subsequently, 20 mL of inoculation cultures were used to inoculate 1 L of LB$_{Cm}$ at 37°C and 180 rpm until an OD$_{600}$ of 0.6–0.8 was reached and induced by addition of 5 mM arabinose. For protein expression the cultures were incubated over night at 37°C and 180 rpm. Cells were pooled and harvested by centrifugation (10.000 xg). Centrifuged cells were resuspended in Buffer A (50 mM sodium phosphate, 300 mM NaCl, 10 mM Imidazole, pH 8.0) and frozen at −80°C. Thawed cells were treated with DNase and lysozyme and incubated for 30 min on a rotary mixer at room temperature. Cell lysis was performed by ultrasonication and the lysate was centrifuged for 1 h at 45000 xg and 4°C and filtered through a 0.45 μm Durapore PVDF membrane (Steriflip, Millipore). The clear lysate was used for further experiments.

Ni-NTA Resin Batch Protein Purification: For purification of the expressed proteins and their ST-SC conjugates Ni-NTA superflow resin (Qiagen, Germany) was used. 10 mL of clear lysate was mixed with 100 μL of Buffer A washed Ni-NTA resin and incubated for 20 min on a spinning wheel. After incubation Ni-NTA resin was sedimented by gravity and washed 2 times with 2 mL Buffer A. For releasing the proteins of the resin 500 μL of Buffer B (50 mM sodium phosphate, 300 mM NaCl, 500 mM Imidazole, pH 8.0) was

Chemistry–A European Journal

Research Article
doi.org/10.1002/chem.202202157

Chemistry
Europe
European Chemical
Societies Publishing

added to the washed resin. The supernatant was used for subsequent DLS-measurements.

Dynamic Light Scattering Measurements: For DLS measurements of purified protein samples 100 μL of purified protein solution was transferred into UV-cuvettes. Loaded cuvettes were placed in a Nano-Series ZetaSizer Nano ZSP (Malvern Instruments, UK) equipped with a He–Ne-Laser (633 nm). Before measurements proteins samples were pre-incubated at 30 °C for 5 min. Subsequently the average hydrodynamic radius of the protein particles (Z-average), calculated from the auto-correlated light intensity data using the ZetaSizer software, was measured.

Atomic Force Microscopy: To visualize inCell-AEH particles, purified protein samples were analyzed by AFM. For sample preparation, proteins were diluted up to 1000-fold in KM-buffer (100 mM potassium phosphate, pH 7.5, 1 mM $MgCl_2$) before adsorbing 10 μL onto a freshly cleaved mica platelet (Plano GmbH) for 10 min at RT. Measurements were performed in liquid Tapping Mode with SNL-10 cantilevers (0.35 Nm-1, Bruker) on a MultiMode™ 8 atomic force microscope (Bruker) equipped with a NanoScope V controller. The scans were processed using NanoScope Analysis software (Bruker). The size distribution of visualized protein particles was calculated as feret diameter using ImageJ.

Toluene Permeabilization of *E. coli* Cells: *E. coli* BL-21 (DE) cells harboring the control or inCell-AEH vectors were inoculated into 30 mL LB_{Cm} and cultivated overnight at 37 °C and 180 rpm. The next day, 2 mL of the cultures were used to inoculate 100 mL LB_{Cm} at 37 °C and 180 rpm until an optical density of 0.6–0.8 was reached. Subsequently the cells were induced with arabinose to a final concentration of 5 mM and incubated overnight at 25 °C and 180 rpm for protein expression and inCell-AEH formation. The induced cells were centrifuged and resuspended in KM-buffer to a final cell density OD_{600} of 10. To permeate the cells, 25 μL of toluene was added to 500 μL of cell suspension and incubated at 4 °C for 30 min. After treatment the cells were washed with KM-buffer. The biocatalytic activity of non- and toluene treated cells was analyzed using the substrate 5-nitrononane-2,8-dione (NDK) **1**. To this end a substrate mix (5 mM NDK **1**, 100 mM glucose, 1 mM $NADP^+$ in KM-buffer) was transferred onto the washed cells and incubated for 20 min at room temperature and 500 rpm shaking. The reaction was quenched using 50 μL 7 M guanidinium chloride mixed with 150 μL of the sample. Subsequently 50 μL of the quenched reaction mix was extracted with 150 μL ethyl acetate and 50 μL of the upper layer was transferred on a 96-well plate. After evaporation of the solvent samples were analyzed by normal phase HPLC.

HPLC Analysis: For HPLC analysis of the substrate NDK **1** and the corresponding reduction products **2a/2b** & **3** a chiral Phenomenex HPLC Lux Cellulose-2 column was used as stationary phase. The mobile phase was run as a mixture of 9:1 n-heptane/2-propanol at a flowrate of 0.5 mL/min and at 10 °C. Educts and products were analyzed by an UV-detector at 210 nm. Retention time of the analytes: ~7.4 min NDK **1**; ~5.7 min (R)-syn hydroxyketone **2a**; ~5.1 min (R)-anti hydroxyketone **2b**; ~3.7 min (R,R)-diol **3** (Figure S2).

Flow Setup for Continuous Biocatalysis: The used flow biocatalysis setup is an assembly of three parts: 1) the substrate stocks, 2) the flow reactors and 3) the sample collection stage. The substrate stocks consisted of 20 mL syringes containing KM-buffer supplemented with 5 mM NDK, 1 mM $NADP^+$ and 100 mM glucose and 0.01% sodium azide. Syringes were installed on a pump unit and connected to the reactors by ⌀ 0.4 mm tubes. The flow bioreactors are milled structures of polytetrafluoroethylene (for dimensions see Figure S3) and contain a chamber that holds a total of 100 μL reaction volume. The construction plan corresponds to a scaled-down version from 200 μL to 100 μL of a reactor previously published by Meng et al.[28] To load and trap the cell suspension inside the reaction chamber, two filter sets were added to the reactor's upper and bottom outlets. Each filter set consisted of 2x cellulose membrane of 5 μm pore size, and in between 2x nitro-cellulose membranes of 0.2 μm pore size. After adding one filter set to the bottom side of the reactor, 100 μL of cell suspension was added inside the chamber then trapped by the second filter set on the top side. The reactors outflow was then automatically collected in a 96-well plate at preset time intervals using a robotic rotaxSYS360 arm (Cetoni, Germany). Flow rate was set to 5 μL*min⁻¹ and the tubes were plugged into the pre-loaded reactors. Samples of 2x reaction volumes (i.e. 200 μL) were collected every 4 h and quenched in with 100 μL of a preloaded 7 M guanidium chloride solution. Eventually, the samples were extracted and analyzed by HPLC.

Immobilization on Epoxide Microparticles: For immobilization of the inCell-AEH out of crude extracts, 15 mg of commercially available epoxide activated microparticles (Profinity Beads, Bio-Rad) were functionalized as previously reported.[29] Subsequently the microparticles were washed in KM-buffer. Finally, the microparticles were suspended in 100 μL KM-buffer and loaded into the reactor chamber.

Conflict of Interest

The authors declare no conflict of interest.

Data Availability Statement

The data that support the findings of this study are available from the corresponding author upon reasonable request.

Keywords: biocatalysis · enzymes · immobilization · microreactors · stereoselective reactions

[1] a) M. B. Quin, K. K. Wallin, G. Zhang, C. Schmidt-Dannert, *Org. Biomol. Chem.* **2017**, *15*, 4260–4271; b) N. Adebar, A. Nastke, H. Gröger, *React. Chem. Eng.* **2021**, *6*, 977–988.

[2] F. S. Aalbers, M. W. Fraaije, *ChemBioChem* **2019**, *20*, 20–28.

[3] S. Schmidt-Dannert, G. Zhang, T. Johnston, M. B. Quin, C. Schmidt-Dannert, *Appl. Microbiol. Biotechnol.* **2018**, *102*, 8373–8388.

[4] V. D. Jäger, M. Piqueray, S. Seide, M. Pohl, W. Wiechert, K.-E. Jaeger, U. Krauss, *Adv. Synth. Catal.* **2019**, *361*, 2616–2626.

Chemistry–A European Journal

Research Article
doi.org/10.1002/chem.202202157

Chemistry Europe
European Chemical
Societies Publishing

[5] S. Kim, J. S. Hahn, *J. Biotechnol.* **2014**, *192*, 192–196.

[6] W. Kang, T. Ma, M. Liu, J. Qu, Z. Liu, H. Zhang, B. Shi, S. Fu, J. Ma, L. T. F. Lai, S. He, J. Qu, S. Wing-Ngor Au, B. Ho Kang, W. C. Yu Lau, Z. Deng, J. Xia, T. Liu, *Nat. Commun.* **2019**, *10*, 4248.

[7] A. Rajendran, E. Nakata, S. Nakano, T. Morii, *ChemBioChem* **2017**, *18*, 696–716.

[8] G. Sachdeva, A. Garg, D. Godding, J. C. Way, P. A. Silver, *Nucleic Acids Res.* **2014**, *42*, 9493–9503.

[9] a) K. S. Rabe, J. Muller, M. Skoupi, C. M. Niemeyer, *Angew. Chem. Int. Ed. Engl.* **2017**, *56*, 13574–13589; b) G. A. Ellis, W. P. Klein, G. Lasarte-Aragones, M. Thakur, S. A. Walper, I. L. Medintz, *ACS Catal.* **2019**, *9*, 10812–10869.

[10] a) H. Lee, W. C. DeLoache, J. E. Dueber, *Metab. Eng.* **2012**, *14*, 242–251; b) C. You, S. Myung, Y. H. Zhang, *Angew. Chem. Int. Ed. Engl.* **2012**, *51*, 8787–8790.

[11] T. Peschke, P. Bitterwolf, S. Gallus, Y. Hu, C. Oelschlaeger, N. Willenbacher, K. S. Rabe, C. M. Niemeyer, *Angew. Chem. Int. Ed. Engl.* **2018**, *57*, 17028–17032.

[12] B. Zakeri, J. O. Fierer, E. Celik, E. C. Chittock, U. Schwarz-Linek, V. T. Moy, M. Howarth, *Proc. Nat. Acad. Sci.* **2012**, *109*, E690–697.

[13] a) P. Bitterwolf, S. Gallus, T. Peschke, E. Mittmann, C. Oelschlaeger, N. Willenbacher, K. S. Rabe, C. M. Niemeyer, *Chem. Sci.* **2019**, *10*, 9752–9757; b) P. Bitterwolf, F. Ott, K. S. Rabe, C. M. Niemeyer, *Micromachines* **2019**, *10*, 783; c) E. Mittmann, S. Gallus, P. Bitterwolf, C. Oelschlaeger, N. Willenbacher, C. M. Niemeyer, K. S. Rabe, *Micromachines* **2019**, *10*, 795.

[14] G. Zhang, M. B. Quin, C. Schmidt-Dannert, *ACS Catal.* **2018**, *8*, 5611–5620.

[15] S. E. Geissinger, A. Schreiber, M. C. Huber, L. G. Stuhn, S. M. Schiller, *ACS Synth. Biol.* **2020**, *9*, 827–842.

[16] Q. Sun, B. S. Heater, T. L. Li, W. J. Ye, Z. H. Guo, M. K. Chan, *Bioconjugate Chem.* **2022**, *33*, 386–396.

[17] W. Dong, H. Sun, Q. Chen, L. Hou, Y. Chang, H. Luo, *Int. J. Biol. Macromol.* **2022**, *199*, 358–371.

[18] a) K. Niefind, J. Muller, B. Riebel, W. Hummel, D. Schomburg, *J. Mol. Biol.* **2003**, *327*, 317–328; b) M. Skoupi, C. Vaxelaire, C. Strohmann, M. Christmann, C. M. Niemeyer, *Chem. Eur. J.* **2015**, *21*, 8701–8705.

[19] W. Hilt, G. Pfleiderer, P. Fortnagel, *Biochim. Biophys. Acta* **1991**, *1076*, 298–304.

[20] L. M. Guzman, D. Belin, M. J. Carson, J. Beckwith, *J. Bacteriol.* **1995**, *177*, 4121–4130.

[21] N. F. Paoni, D. E. Koshland, *Proc. Natl. Acad. Sci. USA* **1979**, *76*, 3693–3697.

[22] T. Peschke, M. Skoupi, T. Burgahn, S. Gallus, I. Ahmed, K. S. Rabe, C. M. Niemeyer, *ACS Catal.* **2017**, *7*, 7866–7872.

[23] Y. Zhang, S. Tsitkov, H. Hess, *Nat. Commun.* **2016**, *7*, 13982.

[24] Y. F. Zhang, H. Hess, *ACS Catal.* **2017**, *7*, 6018–6027.

[25] S. Tsitkov, H. Hess, *ACS Catal.* **2019**, *9*, 2432–2439.

[26] J. E. Dueber, G. C. Wu, G. R. Malmirchegini, T. S. Moon, C. J. Petzold, A. V. Ullal, K. L. Prather, J. D. Keasling, *Nat. Biotechnol.* **2009**, *27*, 753–759.

[27] D. G. Gibson, L. Young, R. Y. Chuang, J. C. Venter, C. A. Hutchison, H. O. Smith, *Nat. Methods* **2009**, *6*, 343-U341.

[28] M. Peng, D. L. Siebert, M. K. M. Engqvist, C. M. Niemeyer, K. S. Rabe, *ChemBioChem* **2021**.

[29] T. Peschke, M. Skoupi, T. Burgahn, S. Gallus, I. Ahmed, K. S. Rabe, C. M. Niemeyer, *ACS Catal.* **2017**, *7*, 7866–7872.